THE JOURNAL OF PHYSICAL CHEMISTRY B

Article

pubs.acs.org/JPCB

Molecular Dynamics Simulations of Quinoline in the Liquid Phase

Jean-Christophe Soetens,*[,†] Norariza Ahmad,[‡] Rohana Adnan,[‡] and Claude Millot*[,§]

[†]UMR CNRS-Université Bordeaux 1 n° 5255, Institut des Sciences Moléculaires, 351, Cours de la Libération, 33405 Talence, France

[‡]School of Chemical Sciences, Universiti Sains Malaysia, 11800 Minden Penang, Malaysia

[§]UMR CNRS-Université de Lorraine n° 7565, Equipe CBT, Faculté des Sciences et Technologies, Boulevard des Aiguillettes, BP 70239, 54506 Vandoeuvre-lès-Nancy Cedex, France

ABSTRACT: Molecular dynamics simulations of liquid quinoline have been performed at experimental densities corresponding to the temperature range 276−320 K. The intermolecular potential is a simple effective two-body potential between rigid molecules having 17 atomic Lennard-Jones and electrostatic Coulomb interaction sites. The vaporization enthalpy is overestimated by 8−9% with respect to the experimental value. The translational diffusion coefficient exhibits a small non-Arrhenius behavior with a change in temperatures near 290 and 303 K. The rotational diffusion tensor is rotated around the z axis perpendicular to the molecular plane by an angle of 4−6° with respect to the frame of reference defined by the principal axes of inertia. The rotational diffusion tensor presents a significant anisotropy with $D_{rot,y}/D_{rot,x} \simeq 0.6-0.5$ and $D_{rot,z}/D_{rot,x} \simeq 1.6-1.3$ between 276 and 320 K when the x axis is defined as the long molecular axis and the y axis is situated nearly along the central C−C bond. The rotational diffusion coefficients, the reorientational correlation times of the C−H vectors, and the T_1 ^{13}C NMR relaxation times present a non-Arrhenius break around 288−290 K in agreement with several experimental results. In addition, a non-Arrhenius break can also be observed at 303 K for these properties. It has been found that the structure evolves smoothly in the studied temperature range. Center of mass−center of mass and atom−atom radial distribution functions show a monotonous evolution with temperature. Various types of first-neighbor dimers have been defined, and their population analysis has revealed a continuous monotonous evolution with temperature. Thus, the non-Arrhenius behavior observed for translational and rotational diffusion is correlated with the monotonous evolution of the population of first-neighbor dimers at a microscopic level and not with a sharp structural transition.

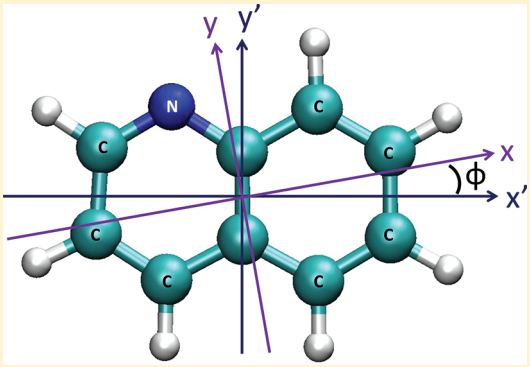

1. INTRODUCTION

The experimental studies of the NMR spin−lattice relaxation times (T_1) of ^{13}C and of the saturated heat capacity of quinoline in the liquid phase by Jalabert et al.[1] have revealed an unusual change in the evolution of these properties at a temperature T_t of 290 K. These studies have extended and confirmed the preliminary results obtained by Zinzius and Lehn[2] about 20 years before. These results reported a change in the temperature dependence of the NMR spin−spin relaxation time T_2 ^{14}N and the NMR spin−lattice relaxation time T_1 ^{2}H and T_1 ^{13}C near the same temperature. Such a change in dynamic behavior has suggested that a continuous structural change in the liquid organization between the melting temperature (T_m) and the transition temperature (T_t) or a change of molecular organization at T_t may occur.[1,3] Such a transition temperature was not observed for isoquinoline.[2] Quinoline and isoquinoline are planar molecules with three different inertia constants (see Figure 1 for the definition of the molecular axes). The rotational diffusion of such molecular systems is very anisotropic, and NMR relaxation data have been used to analyze the anisotropy for quinoline[1,2,4] and for isoquinoline.[2] Using neutron quasielastic scattering, as well as the available information from existing NMR relaxation studies[1] and depolarized light scattering data,[5] Bermejo et al. have shown that only rotational and not translational diffusion coefficients exhibit a deviation from Arrhenius behavior at about 290 K.[4]

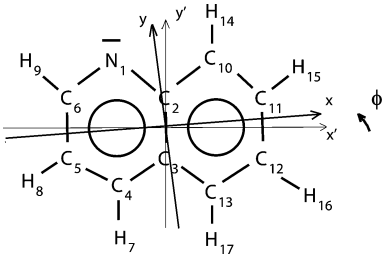

Figure 1. Quinoline molecule in the frame of reference defined by the principal axes of inertia (x',y',z') and orientation of the rotational diffusion tensor (x,y,z). The z and z' axes coincide and are perpendicular to the molecular plane. Numbering of the C−H vectors: C_6−H_9 (CH1); C_5−H_8 (CH2); C_4−H_7 (CH3); C_{13}−H_{17} (CH4); C_{12}−H_{16} (CH5); C_{11}−H_{15} (CH6); C_{10}−H_{14} (CH7).

Received: January 4, 2012
Revised: April 11, 2012
Published: May 4, 2012

   dx.doi.org/10.1021/jp300103b | J. Phys. Chem. B 2012, 116, 5719−5728

Letamendia et al. have observed anomalies at 290 and 315 K for liquid quinoline in the depolarized Rayleigh spectra[6] and also in the sound velocity and in the specific heat capacity ratio C_p/C_v.[7] Moreover, Agnus et al.[8] have found anomalies in the dielectric permittivity of liquid quinoline at 291−292 K and 311−313 K. Robert et al.[9] and Gauthier et al.[10] have observed a transition temperature in NMR relaxation time T_1 of ^{13}C for quinoline, 2-methylquinoline (quinaldine), 4-methylquinoline (lepidine), and 6-methylquinoline, whereas isoquinoline, 7-methylquinoline, quinozaline, and quinoxaline do not display the same property. Quinoline and lepidine have also been studied in the supercooled state;[10] the behavior of relaxation times is regular for quinoline when the plot of $\ln(1/T_1{}^{13}\mathrm{C})$ vs $1/T$ of lepidine presents a maximum around 245 K.

Anomalies in the temperature dependence of the properties of other molecular liquids have been reported. For example, anomalies in the depolarized light scattering of hexafluorobenzene have been reported and considered as the signature of a possible structural change.[11] Later, molecular dynamics simulations of this liquid have not given evidence of any particular structural transition.[12]

In this work, we have explored quinoline using extensive molecular dynamics simulations in the normal liquid phase in the temperature range 276−320 K. Our goal was first to reproduce the rather subtle experimental observations on ^{13}C NMR relaxation times and second to understand this behavior at a microscopic level. In section 2, the molecular dynamics simulations are described in detail. In section 3, the theoretical background behind the calculation of dynamic properties, its links with NMR relaxation measurements, and the modeling of structure at microscopic level are presented. The simulation results are discussed and compared to experimental ones in section 4.

2. SIMULATION DETAILS

The molecules are supposed to be rigid and to interact through an effective atom−atom potential (17 sites per molecule), composed of a Lennard-Jones part and a Coulomb interaction between partial charges. The interaction energy between two molecules i and j is given by

$$E_{ij} = \sum_{a\in i}\sum_{b\in j}\left(\frac{1}{4\pi\varepsilon_0}\right)\frac{q_a q_b}{r_{aibj}} + 4\varepsilon_{ab}\left(\left(\frac{\sigma_{ab}}{r_{aibj}}\right)^{12} - \left(\frac{\sigma_{ab}}{r_{aibj}}\right)^{6}\right) \quad (1)$$

where ε_0 is the vacuum dielectric permittivity and r_{aibj} the distance between atoms a and b. The molecular geometry is obtained by a geometry optimization at the B3LYP/6-31G* level including the reaction field of a polarized dielectric continuum modeled by the PCM model.[13] A static dielectric constant $\varepsilon_{0,\mathrm{RF}}$ of the surrounding solvent equal to 9.03[14] modeling the dielectric constant of liquid quinoline at ambient temperature is used. The electrostatic atomic partial charges q_a are fitted to reproduce the electrostatic potential around a solvated molecule using the Merz−Kollman procedure at the B3LYP/6-31G* level.[14] This calculation takes the solvent effect into account using the PCM model in the same way as for the geometry optimization. These partial charges lead to an electric dipole moment of 2.62 D. A Stark effect measurement has given a value of 2.02 D for the gas phase dipole moment of quinoline.[15] The increased value of the molecular dipole moment with respect to the experimental gas phase value partially corrects the fact that we have not explicitly included the polarizability in the model. The Lennard-Jones parameters σ_{aa} and ε_{aa} are taken from the literature. Three sets have been tested: (i) the Williams−Cox Buckingham parameters[16] for the C−C, N−N, and H−H interactions in aromatic compounds have been transformed into Lennard-Jones sets with the same well depth and distance of zero-potential energy, (ii) the TraPPE parameters,[17] and (iii) the OPLS-AA parameters.[18] In each case, the OPLS combination rules (the geometric mean for σ and ε parameters) have been chosen for interactions involving heteroatomic atom pairs. It should be noted that in the case of the TraPPE parameters the OPLS combination rule for σ underestimates σ_{N-C}, σ_{N-H}, and σ_{C-H} by 0.2, 1.1, and 2.2%, respectively, with respect to the original Lorentz−Berthelot arithmetic combination rule. As the principal aim of this work was to investigate a subtle change in the dynamic properties inside the temperature range 276−320 K, it was important to use a potential that would lead to a realistic pressure at experimental densities or alternatively lead to densities very near the experimental values in constant-pressure, constant-temperature simulations. If these conditions were not fulfilled, it could be argued that an observed change in dynamic behavior vs temperature could be an artifact due to the density or pressure drift with respect to the experimental values. We have chosen to perform NVE simulations at experimental densities, thus our requirement was to obtain a simulated pressure at 276 and 320 K as close to 1 atm as possible as well as a good vaporization enthalpy. Test (i) led to a pressure close to 5000 atm at 276 K and to 3700 atm at 320 K. LJ sets (ii) and (iii) resulted in very similar vaporization enthalpies. The OPLS-AA parameters (iii) provided the best agreement with the experiment for the pressure at 276 and 320 K, and the TraPPE parameters provided pressure about 200 atm larger than the OPLS-AA parameters. Consequently, the OPLS-AA LJ parameters have been regarded as the best compromise when they are used with the B3LYP/6-31G*/PCM Merz−Kollman atomic charges. The Lennard-Jones parameters and atomic electric charges of the model are given in Table 1.

Table 1. Atomic Electric Partial Charges and Lennard-Jones Parameters of the Atom−Atom Effective Intermolecular Potential for Quinoline (See Text and Figure 1)[a]

charges/e	N1	−0.703	C2	0.696	C3	−0.198
	C4	0.064	C5	−0.439	C6	0.372
	H7	0.124	H8	0.192	H9	0.058
	C10	−0.384	C11	−0.072	C12	−0.186
	C13	−0.138	H14	0.174	H15	0.143
	H16	0.152	H17	0.145		
σ/Å	N	3.25	C	3.55	H	2.42
ε/kcal mol^{-1}	N	0.17	C	0.07	H	0.03

[a] $e = 1.6 \times 10^{-19}$ C. 1 kcal = 4.184 kJ.

Molecular dynamics simulations have been carried out at ten experimental densities corresponding to the temperature range 276−320 K on a system composed of N = 216 molecules in a cubic box using periodic boundary conditions. The values of the density have been interpolated from the data of Steele et al.[19] To investigate the system size effect, four simulations at 276, 290, 303, and 320 K have been performed using a system containing N = 1728 molecules. For each density, the production run has been performed in the microcanonical ensemble after a thermalization period stabilizing the temperature.

dx.doi.org/10.1021/jp300103b | J. Phys. Chem. B 2012, 116, 5719−5728

The intermolecular interactions between two molecules have been truncated when the distance between their centers of mass was larger than 17.25 Å (N = 216) or 26 Å (N = 1728), and long-range electrostatic interactions have been taken into account using the Barker−Watts−Neumann reaction field method.[20−22] The dielectric constant of the surrounding continuum has been chosen equal to infinity (conducting boundary condition). The equations of motion have been numerically integrated using the Fincham quaternion algorithm[23,24] with a time step equal to 5 fs during 10 ns (N = 216) or during 1 ns (N = 1728). Velocities have been rescaled every 200 time steps to correct the small energy drift (about 0.05%/ps). A correction has been added to the pressure and the potential energy to compensate for the neglected Lennard-Jones interactions beyond the cutoff distance between centers of mass. This correction has been done while assuming that the center of mass−center of mass molecular radial distribution function was equal to unity when molecules were separated by more than the cutoff distance.[24]

3. CALCULATIONS OF DYNAMIC AND STRUCTURAL PROPERTIES

The translational diffusion coefficient has been obtained from the molecular velocity autocorrelation function (VAC) and from the Einstein relation (MSD).

The rotational diffusion coefficients have been obtained from angular velocity correlation functions (AVCF)

$$D_{\mathrm{rot},a'b'} = \int_0^\infty <\omega_{a',i}(0)\cdot\omega_{b',i}(t) > \mathrm{d}t \tag{2}$$

where $\omega_{a',i}(t)$ is the component of molecular angular velocity around the principal axis of inertia a' of molecule i at time t. In practice, VAC and AVCF have been integrated over 10.22 ps. For symmetrical molecules like benzene (D_{6h} group) in the liquid phase, the rotational diffusion principal axes and the principal axes of inertia coincide; however, for less symmetrical molecules like quinoline (C_s group), they do not necessarily coincide, and a diagonalization of the $D_{\mathrm{rot},a'b'}$ tensor is necessary to get the rotational diffusion coefficients $D_{\mathrm{rot},aa}$, noted $D_{\mathrm{rot},a}$ thereafter. The z axis of the rotational diffusion tensor and the z' inertia axis coincide due to the molecular symmetry of the quinoline molecule. However, the principal axes of rotational diffusion (x,y) are rotated from the principal axes of inertia (x',y') by an angle Φ around the z axis (see Figure 1). The anisotropy of rotational diffusion is accesssible using experimental techniques such as nuclear magnetic relaxation. Moreover, for a planar molecule like quinoline, the rotational diffusion tensor can be completely determined using the combination of several different experiments.[4,25]

NMR relaxation is related to second-order (l = 2) orientational correlation functions $C_m^l(t)$ (even and real functions) of the unit vectors $\mathbf{u}(t)$ linked to the molecules[26−28]

$$C_m^l(t) = <D_{m,0}^l(\theta(0), \varphi(0))D_{m,0}^{l*}(\theta(t), \varphi(t))> \tag{3}$$

where $D_{m,0}^l(\theta(t),\varphi(t))$ are Wigner matrix elements and $(\theta(t),\varphi(t))$ the angles specifying the orientation of the $\mathbf{u}(t)$ vector in space, through spectral densities defined by

$$J_{lm}(\omega) = Re[\int_{-\infty}^{\infty} C_m^l(t)e^{-i\omega t}\mathrm{d}t] \tag{4}$$

calculated at pulsations ω related to the NMR transition frequencies of the spin systems involved in the relaxation mechanisms. If the correlation function is a simple exponential

$$C_m^l(t) = \frac{1}{2l+1}e^{-t/\tau_{lm}} \tag{5}$$

the spectral density is equal to

$$J_{lm}(\omega) = \frac{1}{2l+1}\frac{2\tau_{lm}}{1+(\omega\tau_{lm})^2} \tag{6}$$

and if the time scale of molecular motion is sufficiently small to have $(\omega\tau_{lm})^2 \ll 1$ (extreme narrowing condition), the spectral density of an exponential correlation function becomes equal to $2\tau_{lm}/(2l+1)$.

If the correlation function $C_m^l(t)$ is not an exponential, the correlation time τ_{lm} is defined by

$$\tau_{lm} = (2l+1)\int_0^\infty C_m^l(t)\mathrm{d}t \tag{7}$$

For liquid quinoline, the dominant relaxation mechanism of ^{13}C longitudinal relaxation is the intramolecular $^{13}C-^{1}H$ dipole−dipole mechanism.[3] The corresponding longitudinal relaxation time T_1 involves the J_{2m} of the C−H unit vector and is given by[26]

$$\frac{1}{T_{1,\mathrm{dip}}(^{13}C)} = \frac{3}{4}\left(\frac{\mu_0}{4\pi}\right)^2\frac{\gamma_C^2\gamma_H^2\hbar^2}{r_{CH}^6}\left[2J_{22}(\omega_C+\omega_H)+J_{21}(\omega_C)+\frac{1}{3}J_{20}(\omega_C-\omega_H)\right] \tag{8}$$

In an isotropic medium, $J_{2m}(\omega)$ does not depend on m so that the subscript m can be omitted in the notation of the spectral density and of the correlation times (τ_2). Moreover, within the limit of extreme narrowing, the spectral densities between brackets in eq 8 can be summed up in $4\tau_2/3$.

The structure has been characterized by the molecular radial distribution function between centers of mass

$$g(R) = \frac{<n(R, R+dR)>}{4\pi R^2\rho dR} \tag{9}$$

where $<n(R, R+dR)>$ is the statistical average number of molecules at a distance between R and $R+dR$ from a reference molecule and $\rho = N/V$ the molecular number density. The running coordination number $n(R)$ has then been obtained from

$$n(R) = \int_0^R 4\pi R'^2\rho g(R')\mathrm{d}R' \tag{10}$$

The anisotropy of the first solvation shell around a quinoline molecule has been characterized by defining specific distribution functions in the space regions along the three principal axes of inertia. Taking the z' principal axis, one defines a cylinder of axis z' and of radius R_z, and the distribution function $g_z(Z)$ along the z' axis is defined by

$$g_z(Z) = \frac{<n(Z, Z+dZ)>_{R_z}}{\pi R_z^2\rho dZ} \tag{11}$$

where $<n(Z, Z+dZ)>_{Rz}$ is the statistical average number of molecules within the cylinder of radius R_z and of height dZ at the distance Z along the z' principal axis of inertia of a reference molecule. The distribution functions $g_x(X)$ and $g_y(Y)$ are

dx.doi.org/10.1021/jp300103b | J. Phys. Chem. B 2012, 116, 5719−5728

Table 2. Thermodynamic Properties Obtained from MD Simulations of N Quinoline Molecules and from Experiments[a]

T_{trans}, T_{rot}/K	box edge/Å	ρ/g cm^{-3}	E_{els}	E_{LJ}	E_{pot}	ΔH_{vap}[b]	P
			N = 216				
275.6, 276.6	34.73	1.106	−2.44	−12.83	−15.27	15.8(14.5)	−60
279.4, 280.5	34.76	1.103	−2.42	−12.76	−15.18	15.75(14.45)	−50
284.6, 285.6	34.81	1.098	−2.40	−12.69	−15.09	15.65(14.4)	−60
289.5, 290.6	34.85	1.095	−2.34	−12.63	−14.97	15.55(14.3)	−40
292.6, 293.7	34.87	1.093	−2.34	−12.58	−14.92	15.5(14.25)	−30
297.4, 298.7	34.92	1.088	−2.32	−12.50	−14.82	15.4(14.2)	−40
302.5, 303.7	34.96	1.084	−2.29	−12.42	−14.71	15.3(14.1)	−15
308.5, 309.8	35.01	1.080	−2.26	−12.34	−14.60	15.2(14.0)	−20
314.5, 315.7	35.06	1.075	−2.23	−12.25	−14.48	15.1(13.9)	−20
319.4, 320.5	35.11	1.070	−2.20	−12.18	−14.38	14.95(13.85)	−15
			N = 1728				
276.0, 276.0	69.46	1.106	−2.44	−12.82	−15.26	15.8(14.5)	−70
289.9, 290.0	69.70	1.095	−2.36	−12.61	−14.97	15.55(14.3)	−40
303.2, 303.4	69.92	1.084	−2.29	−12.41	−14.70	15.3(14.1)	−15
320.0, 320.0	70.21	1.070	−2.20	−12.17	−14.37	15.0(13.85)	−10

[a]Energies in kcal mol^{-1}. Pressure in 10^5 Pa. [b]The data between brackets are a linear interpolation of experimental ΔH_{vap} in the range 260−360 K from ref 19.

defined similarly with respect to the principal axes of inertia x' and y'. The radii R_z and R_y have been chosen equal to 3 Å and R_x equal to 2 Å. Due to the planar symmetry of the quinoline molecule, $g_z(Z)$ is equal to $g_z(-Z)$.

The molecular radial distribution function $g(R)$ allows us to define a first solvation shell that is spherical. For anisotropic molecules like quinoline, the distribution functions $g_x(X)$, $g_y(Y)$, and $g_z(Z)$ allow us to represent the first solvation shell in a more realistic way by an ellipsoid with the radii a, b, and c defined by the distance of the first minimum of the functions $g_x(X)$, $g_y(Y)$, and $g_z(Z)$, respectively. For the directions x' or y', the largest of the two values along the $\pm x'$ or $\pm y'$ directions have been chosen for a or b, respectively. To define specific dimer types, regions are defined within the ellipsoidal first solvation shell surrounding the central molecule. Starting from the central molecule in the reference frame defined by the principal axes of inertia (x',y',z') (Figure 1), six F (face) regions have been defined by cones. Each cone has been defined by its summit located at the center of mass of the central molecule, its axis pointing toward $+z'$ (F1), $-z'$ (F2), $+x'$ (F3), $-x'$ (F4), $+y'$ (F5), and $-y'$ (F6) and its opening angle as the angle α on one side of the central axis. Eight S (summit) regions have been defined in a similar way as pointing in the directions of the summits of the parallelepiped that circumscribes the ellipsoid containing the first solvation shell, i.e., S1 (along $+z'$,$+x'$,$+y'$), S2 ($+z'$,$-x'$,$+y'$), S3 ($+z'$,$-x'$,$-y'$), S4 ($+z'$,$+x'$,$-y'$), S5 ($-z'$,$+x'$,$+y'$), S6 ($-z'$,$-x'$,$+y'$), S7 ($-z'$,$-x'$,$-y'$), and S8 ($-z'$,$+x'$,$-y'$). A given F or S dimer type is counted every time the second molecule within the first solvation shell is inside the associated cone, independently from its relative orientation in space.

Due to molecular planar symmetry, the F1 and F2 regions have the same population as well as the summit regions that are associated two by two ($+z'$ and $-z'$, with the same orientations along the x' and y' directions). To count a maximum number of dimers from the first solvation shell and to avoid the double counting of dimers such as S and F (because of the possible overlap between S and F regions), for the angle α a value of 27.5° has been chosen.

In each F or S region, we have also distinguished the orientations by using parallel (P) or perpendicular (T) molecular planes with an angular deviation with respect to perfect orientation that is smaller than an arbitrarily chosen angle equal to α, leading to the dimers called FP, FT, SP, and ST.

4. RESULTS AND DISCUSSION

4.1. Thermodynamics. For each density ρ, Table 2 gives the size of the box containing the sample of N = 216 or N = 1728 molecules and the temperature of each run obtained by averaging the kinetic (translational and rotational) energy. The translational and rotational kinetic energies range from 0.82 kcal mol^{-1} at 276 K to 0.95 kcal mol^{-1} at 320 K.

At each temperature, the molar vaporization enthalpy is derived from the potential energy E_{pot} of the liquid by

$$\Delta H_{vap} = -E_{pot} + RT \quad (12)$$

with R being the perfect gas constant. The statistical averages of potential energy (and van der Waals and electrostatic parts E_{LJ} and E_{els}), of vaporization enthalpy, and of pressure are reported in Table 2. Dividing each MD run in five subruns, the standard deviation is about 0.01 kcal/mol for the potential energy and evolves from 30 × 10^5 Pa at 276 K to 10 × 10^5 Pa at 320 K for the pressure. The vaporization enthalpy is also compared to an experimental determination[19] in Table 2. Though the simulation overestimates the vaporization enthalpy by about 8−9%, the evolution with temperature is well reproduced. For N = 216, the corrective term due to the cutoff of Lennard-Jones interactions varies from −0.18 to −0.17 kcal mol^{-1} for the potential energy and from −130 to −120 × 10^5 Pa for the pressure between 276 and 320 K. For N = 1728, these corrections at the four temperatures are −0.03 kcal mol^{-1} and −20 × 10^5 Pa, respectively.

4.2. Translational Diffusion. The values of the diffusion coefficient between 276 and 320 K are presented in Table 3 and Figure 2. D_{trans} presents a clear break in the Arrhenius plot at 290 K, and a second break near 303 K is also visible mainly from $D_{trans,VAC}$. Uncertainties on $D_{trans,VAC}$ range from ±0.0002 (lowest temperatures) to ±0.0006 Å^2 ps^{-1} (highest temperatures) for N = 216 and remain around ±0.0005 Å^2 ps^{-1} at the four temperatures for the case N = 1728. A comparison is made with the experimental determination by neutron scattering by Bermejo et al.,[4] and the numerical values of the best Arrhenius fit of the experimental D_{trans} proposed by these authors are also

dx.doi.org/10.1021/jp300103b | J. Phys. Chem. B 2012, 116, 5719−5728

Table 3. Translational Diffusion Coefficient ($Å^2$ ps^{-1}) of Liquid Quinoline from MD Simulations and Experiments

T/K	D_{trans} MD (MSD)	D_{trans} MD (VAC)	D_{trans} exp.[a]
	$N = 216$		
276	0.0038	0.0084	0.0225
280	0.0046	0.0099	0.0241
285	0.0058	0.0116	0.0264
290	0.0077	0.0140	0.0287
293	0.0088	0.0154	0.0303
298	0.0105	0.0174	0.0329
303	0.0133	0.0209	0.0355
309	0.0164	0.0236	0.0390
315	0.0203	0.0279	0.0427
320	0.0242	0.0311	0.0457
	$N = 1728$		
276	0.0042	0.0090	0.0225
290	0.0087	0.0149	0.0287
303	0.0130	0.0223	0.0355
320	0.0230	0.0344	0.0457

[a]Best Arrhenius fit of experimental data in the range 260−310 K from ref 4.

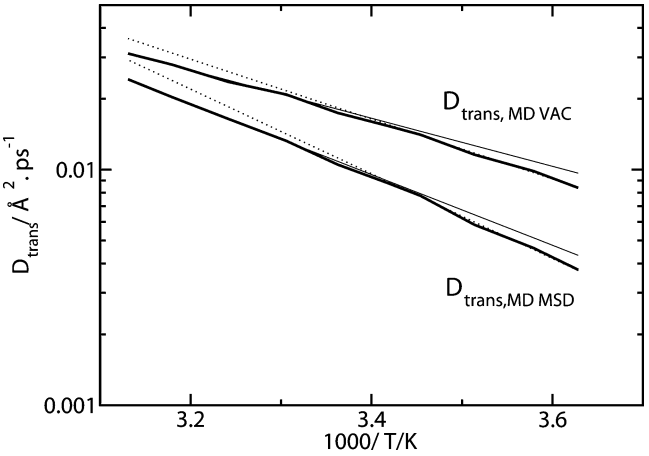

Figure 2. Translational diffusion coefficient ($Å^2$ ps^{-1}) of liquid quinoline as a function of temperature (K) obtained with MD simulations. The thin solid and dotted lines correspond to Arrhenius fits at the highest and lowest temperatures, respectively.

given in Table 3 for comparison. Indeed, the examination of the experimental diffusion coefficient values in Bermejo and co-workers' paper shows that this property presents a slight but noticeable deviation from Arrhenius behavior within this temperature range around 275−290 K.[29] The activation energies fitted from the experimental D_{trans}[4] are 3.0 and 2.65 kcal mol^{-1} at the lowest and highest temperatures, respectively. Our simulations lead to a more pronounced break. From $D_{trans,MSD}$, activation energies of 8.2 and 6.9 kcal mol^{-1} are obtained using the simulation results at the four lowest and highest temperatures, respectively. Using $D_{trans,VAC}$, both activation energies are 5.8 and 4.7 kcal mol^{-1}, respectively. The fact that the simulated values of the diffusion coefficient are lower than the experimental ones and that the activation energy in Arrhenius plots of this property is exaggerated is consistent with the overestimation of the cohesive energy.

4.3. Rotational Diffusion. The values of the diffusion coefficients between 276 and 320 K are presented in Table 4 and Figure 3. The rotational diffusion tensor has first been

Table 4. Rotational Diffusion Coefficients (10^{-3} rad^2 ps^{-1}) of Liquid Quinoline from MD Simulations and Experiments (Data between Brackets Interpolated from Ref 4) and Parameters D_0 (rad^2 ps^{-1}) and E_0 (kcal mol^{-1}) from Arrhenius Fits[a]

T/K	$D_{rot,x}$	$D_{rot,y}$	$D_{rot,z}$	Φ/°
		$N = 216$		
276	3.8 (2.1)	2.1 (1.1)	6.0 (4.3)	4.9
280	4.4 (2.5)	2.35 (1.2)	6.7 (4.9)	4.7
285	5.15 (2.9)	2.65 (1.4)	7.7 (5.9)	5.0
290	6.15 (3.2)	3.1 (1.6)	8.9 (6.6)	4.9
293	6.6 (3.5)	3.35 (1.8)	9.5 (7.1)	4.2
298	7.7 (4.1)	3.75 (2.05)	10.5 (8.1)	4.8
303	8.9 (4.5)	4.30 (2.2)	12.0 (9.1)	4.8
309	10.1 (5.2)	4.85 (2.65)	13.4 (10.5)	4.3
315	11.7 (5.9)	5.55 (2.95)	15.3 (11.9)	4.4
320	13.0 (6.6)	6.15 (3.2)	16.8 (13.2)	4.6
		$N = 1728$		
276	3.7 (2.1)	2.05 (1.05)	5.8 (4.3)	4.1
290	6.1 (3.2)	3.05 (1.65)	8.7 (6.6)	6.4
303	8.7 (4.5)	4.25 (2.2)	11.9 (9.2)	4.6
320	12.9 (6.6)	6.2 (3.2)	16.8 (13.2)	3.8
		Single Arrhenius Fit		
D_0	23.287	5.083	10.007	
E_0	4.767	4.279	4.068	
		$T \leq 290$ K Arrhenius Fit		
D_0	50.373	7.804	18.988	
E_0	5.211	4.524	4.433	
		$T \geq 293$ K Arrhenius Fit		
D_0	15.405	4.443	8.580	
E_0	4.509	4.195	3.973	

[a]Φ is the rotation angle around the molecular z' axis required to obtain the rotation diffusion axes (x,y) from the principal axes of inertia (x',y').

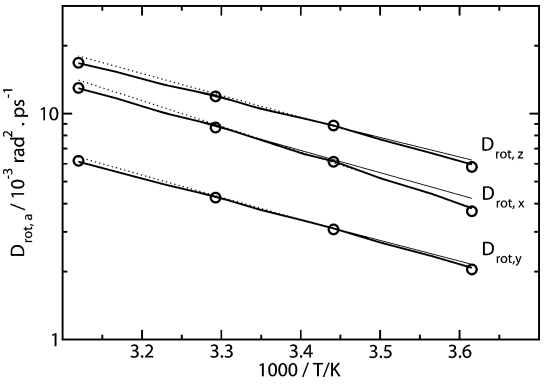

Figure 3. Rotational diffusion coefficients (10^{-3} rad^2 ps^{-1}) of liquid quinoline as a function of temperature (K) obtained with MD simulations. The solid curves go through the simulation results with $N = 216$, and the circles are the results of the four simulations with $N = 1728$. The thin solid and dotted lines correspond to Arrhenius fits at the highest and lowest temperatures, respectively.

computed in the reference frame defined by the principal axes of inertia (x',y',z') and then diagonalized by performing a rotation of the Φ angle around the z' axis. The Φ angle is found to be in the range 4−6° with a weak temperature dependence, which is in good agreement with the experimental results that give Φ in the 3−4° range.[4] Between 276 and 320 K, the uncertainties on D_{rot} (in 10^{-3} rad^2 ps^{-1}) range from ±0.1 to ±0.2

dx.doi.org/10.1021/jp300103b | J. Phys. Chem. B 2012, 116, 5719−5728

for $D_{rot,x}$ and $D_{rot,z}$ and from ±0.05 to ±0.1 for $D_{rot,y}$. The comparison between various experimental determinations of the rotational diffusion constants shows that there is no consensus.[2−4] As regards the ordering of the three rotational diffusion coefficients, molecular dynamics simulations show that $D_{rot,z} > D_{rot,x} > D_{rot,y}$ at each temperature in the studied range. This agrees with the result of ref 4 yielding three different rotational diffusion coefficients $D_2 > D_1 > D_3$ at all temperatures between 276 and 320 K, implying that $(x,y,z) = (1,3,2)$.

As far as the numerical values of the rotational diffusion coefficients are concerned, there are important discrepancies between the different experimental determinations as well as with the MD simulation results. Experimentalists assume that the anisotropic diffusion model is valid to deduce the correlation times from the relaxation times using different fitting techniques. An inaccurate intermolecular potential creates errors in the MD estimation of the dynamic properties. For example, at 303 K, ($D_{rot,z}$, $D_{rot,x}$, $D_{rot,y}$) (in rad^2 ps^{-1}) are equal to (0.0243, 0.0170, 0.0071) for Zinzius,[2] (0.0365, 0.0028, 0.0028) for Jalabert et al.,[3] and (0.0091, 0.0046, 0.0024) for Bermejo et al.,[4] and we obtain (0.0120, 0.0089, 0.0043) with our simulations.

The anisotropy of rotational diffusion as measured through the ratio of rotational diffusion $D_{rot,a}$ ($a = x,y,z$) is found to be important. In our MD simulations, $D_{rot,y}/D_{rot,x}$ varies from 0.55 to 0.47 when the temperature increases from 276 to 320 K, whereas the experimental results show that this quantity increases from 0.5 to 0.6 in this temperature range.[4] Moreover, $D_{rot,z}/D_{rot,x}$ varies from 1.56 to 1.29 when the temperature increases from 276 to 320 K, whereas the experimental results show that this ratio is close to 2.0 with no temperature dependence.[4]

The principal rotational diffusion coefficients $D_{rot,a}$ ($a = x,y$) present a marked deviation from a pure Arrhenius behavior at the temperature 290 K and a less marked one around 303 K. Similarly, $D_{rot,z}$ presents two break temperatures at 288 and 303 K. For $D_{rot,y}$, two changes can be observed around 288 and 303 K, but the non-Arrhenius effect is much weaker than for the other two rotational diffusion constants. These observations, which are reported in Figure 3, are in good agreement with the experimental results of Bermejo and co-workers[4] reproduced in Figure 4. The effects of the system size can also

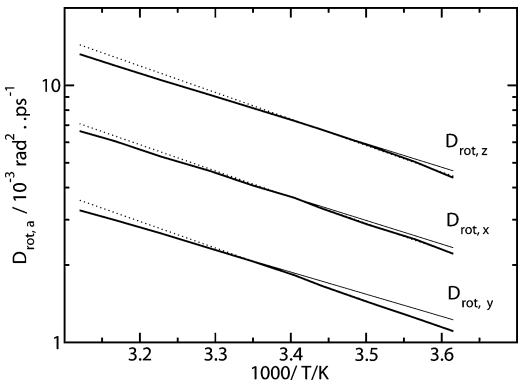

Figure 4. Rotational diffusion coefficients (10^{-3} rad^2 ps^{-1}) of liquid quinoline as a function temperature (K) obtained with NMR relaxation experiments (ref 4). The thin solid and dotted lines correspond to Arrhenius fits at the highest and lowest temperatures, respectively.

be seen in Figure 3. It appears that the rotational diffusion constants are very similar for $N = 216$ and $N = 1728$. The four simulations with $N = 1728$ confirm the non-Arrhenius effect observed with $N = 216$.

A single Arrhenius fit of $D_{rot,a} = D_0 e^{-E_0/RT}$ between 276 and 320 K as well as the Arrhenius fits below and above 290 K are presented in Table 4. Beyond 290 K, the activation energy decreases by 0.70, 0.33, and 0.46 kcal mol^{-1} for $D_{rot,x}$, $D_{rot,y}$, and $D_{rot,z}$, respectively. The corresponding experimental decreases in activation energies obtained by fitting the temperature behavior of the rotational diffusion coefficients in ref 4 are 0.46, 0.77, and 0.54 kcal mol^{-1} (see Figure 4) and in ref 3 are 1.6, 3.0, and 0.6 kcal mol^{-1}, respectively.

4.4. Reorientational Correlation and T_1 ^{13}C NMR Relaxation Times. The reorientational correlation times τ_1 and τ_2 of each C−H vector and of the molecular z axis perpendicular to the molecular plane have been obtained by fitting the correlation function to a linear combination of a Gaussian and two exponential functions. The results are given in Table 5. Dividing the MD runs in four subruns, the standard deviation evolves from ≃5% at 276 K to ≃3% at 320 K for the τ_1 and from ≃4% at 276 K to ≃2% for the τ_2. The τ_1 and τ_2 correlation times for the C−H vectors are also presented in Figures 5 and 6, which show a non-Arrhenius behavior correlated to the behavior of the rotational diffusion coefficients. From the τ_2 correlation times of the C−H vectors, the longitudinal relaxation times T_1 of ^{13}C are obtained assuming that the ^{13}C−^{1}H dipole−dipole intramolecular relaxation mechanism is dominant and that the extreme narrowing condition is valid. Considering experiments operating at 300 MHz for ^{1}H and 75 MHz for ^{13}C resonances[10] as well as the longest τ_2 obtained in our simulation which is approximately 90 ps at 276 K, we have obtained the highest value for $(\omega\tau_2)^2$ occurring in spectral densities equal to 0.045. This gives an error of about 5% in the spectral density if we neglect the frequency dependence. A comparison with experiment[1] shows that our simulations underestimate the results by a factor of 2−3 for the T_1 ^{13}C, and the reorientational correlation times τ_2 are overestimated by the same factor. The inaccuracy of the reorientational correlation times in our simulations is due to deficiencies in the intermolecular potential energy function and the use of a rigid molecular model. The sensitivity of simulated properties to the details of the force field has been analyzed in liquid benzene at ambient conditions.[30] For seven force fields of the literature, the reorientational correlation time τ_2 has been found in the range 1.1−2.5 ps for in-plane vectors and in the range 1.4−6.2 ps for the vector perpendicular to the molecular plane. These observations show how the details of the potential energy surface can significantly affect the molecular reorientation in the liquid phase. An attempt to improve the force field for quinoline would require an extensive analysis of dimer interaction energy using a high-level ab initio method.

At the lowest temperatures, the extreme narrowing hypothesis introduces a small error into our MD estimation of the T_1 ^{13}C. However, we intend to analyze the small non-Arrhenius effect observed experimentally with correlation times 2−3 times shorter than those obtained with our MD simulations[1] and for which the extreme narrowing condition is valid from 276 to 320 K. To do that, we thought it was more appropriate to compute the spectral densities using this assumption to avoid attributing a possible non-Arrhenius behavior to an artifactual frequency dependence of the spectral densities.

The MD results of the NMR T_1 ^{13}C are given in Table 6. Figure 7 presents a plot of $\ln(T_1)$ as a function of inverse temperature and presents two changes in the slope at about

dx.doi.org/10.1021/jp300103b | J. Phys. Chem. B 2012, 116, 5719−5728

Table 5. First-Order τ_1 and Second-Order τ_2 Reorientational Correlation Times (ps) of the C−H Vectors and of the Vector Perpendicular to the Molecular Plane of Liquid Quinoline vs Temperature (K)

T/K	CH1	CH2	CH3	CH4	CH5	CH6	CH7	z axis
				τ_1				
N = 216								
276	200	214	166	166	204	210	166	320
280	170	181	142	141	173	178	141	262
285	140	149	117	117	143	147	117	219
290	112	120	93	93	114	118	92	170
293	102	109	84	84	104	107	84	154
298	88	94	73	73	90	93	73	130
303	73	79	61	60	75	78	60	108
309	63	68	52	52	64	67	52	91
315	54	58	45	45	53	57	45	77
320	49	52	40	40	50	52	40	68
N = 1728								
276	199	212	167	166	203	209	166	313
290	115	123	96	96	117	121	96	169
303	75	80	62	62	77	79	62	107
320	48	52	39	39	49	51	39	67
				τ_2				
N = 216								
276	83	91	64	64	85	89	64	123
280	69	76	53	53	71	74	53	101
285	56	63	44	44	58	61	44	83
290	44	49	34	34	46	48	34	64
293	40	45	30.8	30.8	42	44	30.7	58
298	34	37.7	26.0	25.9	35	36.7	25.9	49
303	28.1	31.3	21.5	21.4	29.1	30.5	21.4	39.3
309	24.0	26.7	18.3	18.3	24.9	26.0	18.3	33.2
315	20.3	22.7	15.5	15.5	21.0	22.1	15.5	27.9
320	18.1	20.2	13.8	13.8	18.8	19.7	13.7	24.6
N = 1728								
276	81	90	64	64	84	88.0	64	120
290	46	51	35	36	47	49.8	35	64
303	28.4	31.6	21.8	21.7	29.4	30.8	21.7	39.7
320	18.0	20.1	13.8	13.7	18.6	19.5	13.7	24.4

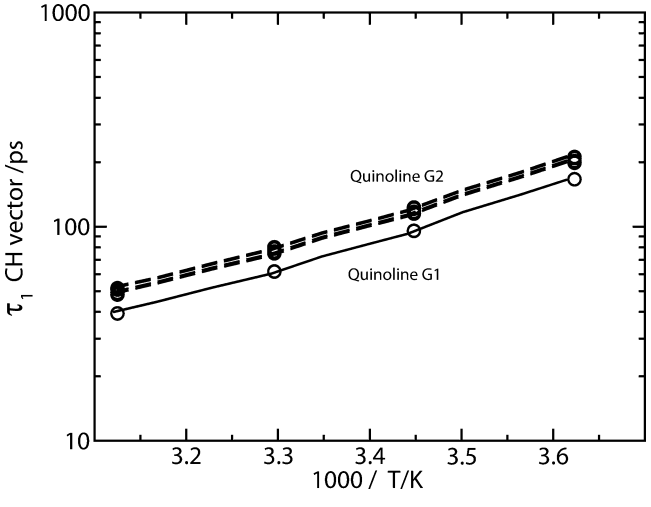

Figure 5. First-order reorientational correlation time τ_1 (ps) of the C−H vectors of liquid quinoline from MD simulations as a function of temperature (K). The reorientational correlation functions are fitted to the linear combination of a Gaussian and two exponential functions. The solid lines correspond to CH3, CH4, and CH7 vectors (G1 group) and the dashed lines to CH1, CH2, CH5, and CH6 vectors (G2 group) (see Figure 1).

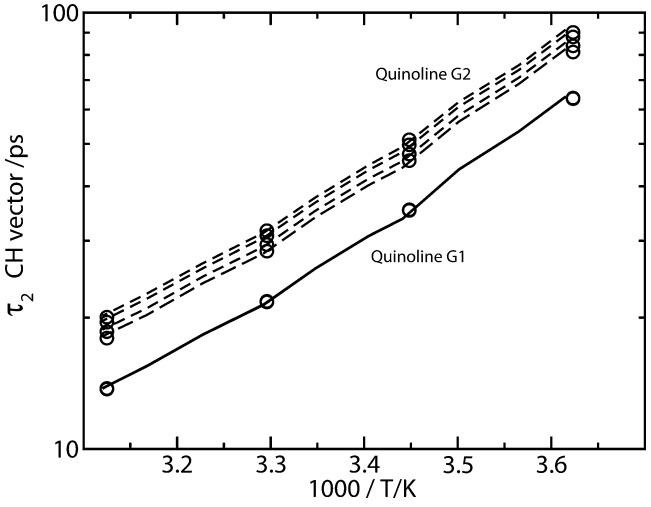

Figure 6. Similar to Figure 5 for the second-order reorientational correlation time τ_2 (ps) of the C−H vectors of liquid quinoline.

290 and 303 K that parallells the behavior of the rotational diffusion coefficients. This plot divides the C−H vectors into two groups: in the first group (G1), the three C−H vectors CH3, CH4, and CH7 are nearly parallel to the y' axis, and in the

dx.doi.org/10.1021/jp300103b | J. Phys. Chem. B 2012, 116, 5719−5728

Table 6. MD Estimation of NMR Longitudinal Relaxation Time of ^{13}C (s) in Liquid Quinoline[a]

T/K	CH1	CH2	CH3	CH4	CH5	CH6	CH7
276	0.55	0.49	0.70	0.70	0.52	0.50	0.70
280	0.66	0.59	0.84	0.85	0.63	0.61	0.84
285	0.81	0.71	1.03	1.03	0.77	0.73	1.02
290	1.03	0.90	1.34	1.34	0.98	0.93	1.33
293	1.13	1.00	1.46	1.47	1.07	1.03	1.45
298	1.34	1.18	1.74	1.74	1.27	1.22	1.72
303	1.62	1.42	2.10	2.11	1.54	1.47	2.09
309	1.89	1.67	2.46	2.47	1.80	1.72	2.44
315	2.24	1.96	2.91	2.92	2.13	2.02	2.89
320	2.50	2.21	3.28	3.28	2.39	2.28	3.25

[a]Pure intramolecular dipolar mechanism (between carbon atom and covalently bound hydrogen atom) and extreme narrowing conditions are assumed.

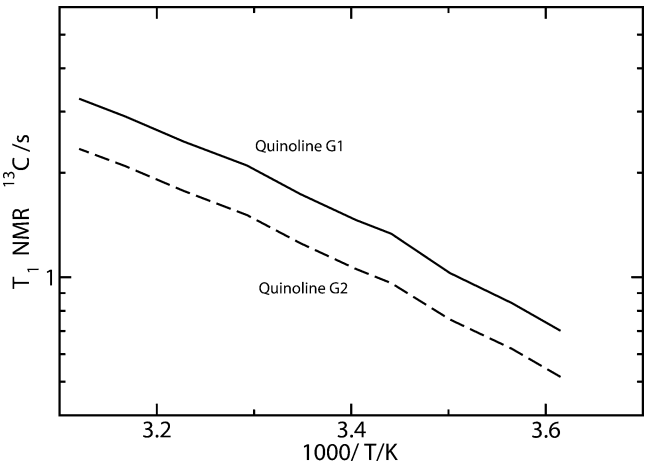

Figure 7. Molecular dynamics simulation of the NMR longitudinal relaxation time T_1 (s) of ^{13}C of liquid quinoline as a function of temperature (K). Dipolar $^{13}C-^{1}H$ mechanism and extreme narrowing are assumed. Solid curve: average of T_1 over the G1 group (CH3, CH4, and CH7). Dashed curve: average of T_1 over the G2 group (CH1, CH2, CH5, and CH6).

second one (G2), the four C−H vectors CH1, CH2, CH5, and CH6 make an angle of approximately 60° with the y' axis. The break at 290 K reproduces the experimental break observed by Zinzius[2] at 286 K (group G2) and 292 K (group G1) and others at 290 K[1,3]and 285 K[9] in a qualitative way. The NMR relaxation measurements have not displayed the second break around 303 K, but an anomaly in the depolarized Rayleigh spectrum[6] and in the dielectric permittivity[8] has been observed around 311−315 K.

Chemical shift anisotropy is the second important relaxation mechanism involved in the ^{13}C longitudinal nuclear magnetic relaxation of quinoline. Experiments have shown that its contribution to T_1 ^{13}C represents 1/15 of the contribution of the dipolar mechanism.[3] Taking this contribution into account will be useful for a quantitative comparison with experimental data once simulation results using a more accurate force field are available.

4.5. Structure. Figure 8 (top) presents the evolution of the radial distribution function (rdf) between centers of mass with temperature, which appears to be monotonous. By integrating this function up to 8.75 Å, one obtains a coordination number in the spherical first shell decreasing from approximately 13.4

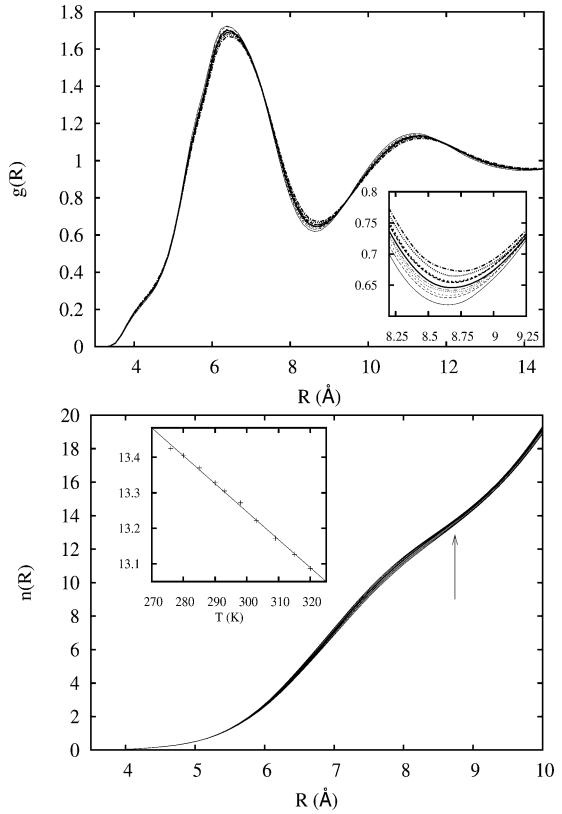

Figure 8. Top: Radial distribution function $g(R)$ between centers of mass vs R (Å) at 10 temperatures in the range 276−320 K. The inset presents an enlargement of the curves around the distance corresponding to the first minimum. Bottom: Coordination number $n(R)$ vs R obtained from integration of $g(R)$. The inset presents the coordination number for R = 8.75 Å as a function of temperature.

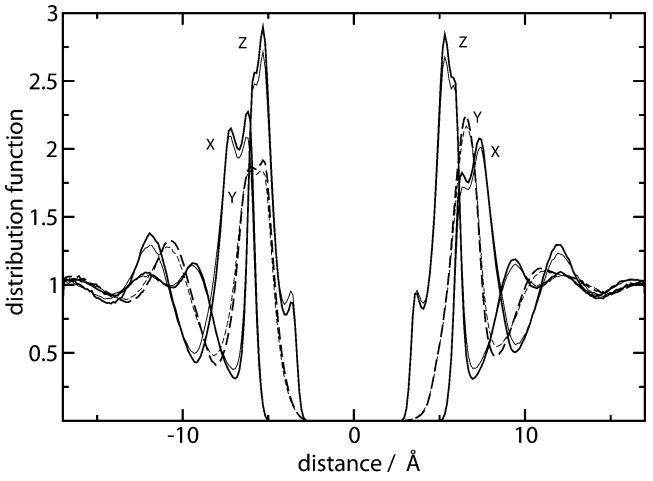

Figure 9. Distribution functions $g_x(X)$, $g_y(Y)$, and $g_z(Z)$ of liquid quinoline. The reference central molecule has the orientation shown in Figure 1. Molecules are counted within cylinders of radius 2, 3, and 3 Å along the x', y', and z' directions, respectively. Thick and thin curves correspond to 276 and 320 K, respectively.

molecules at 276 K to 13.1 molecules at 320 K (see Figure 8 (bottom)). The examination of the atom−atom rdfs $g_{ab}(r)$ shows that these functions also evolve monotonously with temperature. The examination of the location and the intensity of the first maximum of the various atom−atom rdf's at different temperatures has not revealed any particular change

dx.doi.org/10.1021/jp300103b | J. Phys. Chem. B 2012, 116, 5719−5728

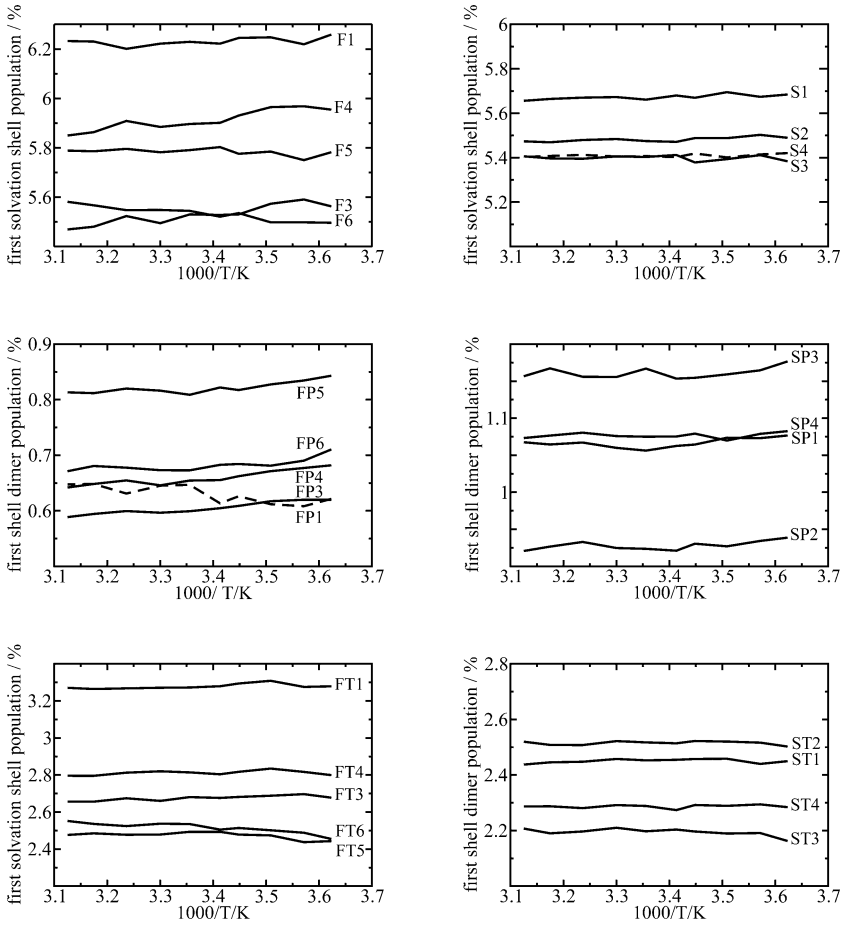

Figure 10. Evolution with temperature of the population of first solvation shell dimer types defined in the text. Top left: face dimers (F2 dimer is equivalent to F1 by symmetry). Top right: summit dimers (by symmetry, S5, S6, S7, and S8 are equivalent to S1, S2, S3, and S4, respectively). Center left: face dimers with mainly parallel molecular planes. Center right: summit dimers with mainly parallel molecular planes. Bottom left and right: same as center left and right for the perpendicular dimers, respectively.

near 290 or 303 K. The analysis of the variation of the atom−atom rdf's $\Delta g_{ab}(r)/\Delta T$ due to a jump of temperature ΔT (from 3 to 6 K in our simulations) has led to the observation of some accidents occurring at different temperatures according to the chosen rdf. It was impossible to define a transition temperature from these observations.

Figure 9 presents the distribution functions $g_x(X)$, $g_y(Y)$, and $g_z(Z)$ defined in the previous section at 276 and 320 K. Thanks to these curves, one can define the first solvation shell around a reference molecule as an ellipsoid rather than a sphere. From the position of the first minimum of these distribution functions, it has been deduced that an ellipsoid with a = 9.55 Å, b = 8.40 Å, and c = 7.15 Å includes the first solvation shell at all temperatures in the range 276−320 K. The average population of first neighbors in this ellipsoid evolves from 12.3 at 276 K to 11.9 at 320 K.

Figure 10 presents the temperature evolution of the different dimer type populations within the ellipsoidal first shell. We have found that all the chosen types of first-neighbor dimers evolve regularly with temperature, and no sharp modification has been observed. It can be noted that the F3 and F6 curves cross at approximately 290 K, which is the temperature of the break for T_1 ^{13}C. Other crossings can be observed. The regular temperature evolution of the structure at the microscopic level is correlated with the evolution of the thermodynamic and dynamic properties.

According to the definition, the S and F dimers represent about 44% and 35% of the dimers of the first shell at all temperatures. The total parallel (P) and perpendicular (T) relative orientations amount to 10.4% and 35.7% at 276 K and to 10.2% and 35.9% at 320 K, respectively. The population ratio T/P thus evolves from 3.4 at 276 K to 3.5 at 320 K.

5. CONCLUSION

Molecular dynamics simulations of liquid quinoline between 276 and 320 K have been presented in detail. The main results concern the analysis of molecular rotational diffusion and confirm the experimental observations of a change in the temperature evolution of NMR relaxation times T_1 ^{13}C around 285−290 K made by different groups. A change in behavior of the Arrhenius plot of the rotational diffusion coefficients, of the reorientational correlation times of the C−H vectors, and of the T_1 ^{13}C has been found in our simulations around T_t = 290 K. Another change has also been observed around T_t = 303 K. It has been found that these changes of behavior of dynamic properties are essentially due to the natural temperature dependence of the dynamical properties and linked to the continuous evolution of the structure. The breaks in the Arrhenius plot can be explained by the monotonous continuous evolutions of different dimer type populations in the first solvation shell. This is in agreement with the idea of a continuous change in the liquid organization between the melting temperature T_m and T_t.[1] Indeed, the

dx.doi.org/10.1021/jp300103b | J. Phys. Chem. B 2012, 116, 5719−5728

simulations show that at first-neighbor dimer level the liquid structure has the same regular evolution below and above T_t. To our knowledge, our work is the first extensive molecular dynamics study on this molecular system. The comparison between the simulation and the experimental results has revealed that the intermolecular potential overestimates the cohesive energy and that the translational and rotational molecular diffusion are slowed down with respect to the experimental observations. Correcting these artifacts by including flexibility, polarizability, and quantum corrections for hydrogen motions while keeping a sufficient statistical sampling is possible and would be a significant improvement.

AUTHOR INFORMATION

Corresponding Author

*E-mail: jc.soetens@ism.u-bordeaux1.fr. Tel.: ++33 (0)5 40 00 22 42. Fax: ++33 (0)5 40 00 84 02. E-mail: claude.millot@univ-lorraine.fr. Tel.: ++33 (0)3 83 68 43 84. Fax: ++33 (0)3 83 68 43 71.

Notes

The authors declare no competing financial interest.

ACKNOWLEDGMENTS

We thank the University of Lorraine, the University of Bordeaux 1, the CNRS, the French Embassy in Kuala Lumpur, and the Universiti Sains Malaysia (FRGS grant 203/PKIMIA/6711147 and USM-IPS grant 308/AIPS/414501) for their financial support. Computer time for this study was provided by MCIA (Mésocentre de Calcul Intensif Aquitain), the public research HPC centre in Aquitaine. C.M. thanks D. Canet for useful discussions and D. Vanneste and L. Gauthier for their interest in the early stage of this work.

REFERENCES

(1) Jalabert, D.; Robert, J. B.; Roux-Buisson, H.; Kintzinger, J. P.; Lehn, J. M.; Zinzius, R.; Canet, D.; Tekely, P. *Europhys. Lett.* **1991**, *15*, 435.
(2) Zinzius, R. *Etude de la dynamique moléculaire de la quinoléine et de l'isoquinoléine par relaxation nucléaire*; Thèse de 3e cycle, University Louis Pasteur: Strasbourg, France, 1972.
(3) Jalabert, D.; Robert, J. B.; Canet, D.; Tekely, P. *Mol. Phys.* **1993**, *79*, 673.
(4) Bermejo, F. J.; Garciá-Hernández, M.; Howells, W. S.; Burriel, R.; Mompeán, F. J.; Martin, D. *Phys. Rev. E* **1993**, *48*, 2766.
(5) Stegeman, G. I. A.; Stoicheff, B. P. *Phys. Rev. A* **1973**, *7*, 1160.
(6) Letamendia, L.; Belkadi, M.; Eloutassi, O.; Pru-Lestret, E.; Nouchi, G.; Rouch, J.; Blaudez, D.; Mallamace, F.; Micali, N.; Vasi, C. *Phys. Rev. E* **1996**, *54*, 5327.
(7) Letamendia, L.; Belkadi, M.; Eloutassi, O.; Rouch, J.; Risso, D.; Cordero, P.; Patashinski, A. Z. *Phys. A* **2005**, *354*, 34.
(8) Agnus, B.; Ellison, W.; Vicq, G.; Delbos, G. *C. R. Acad. Sci. Paris* **1997**, *324*, *Série IIb*, 331.
(9) Robert, J. B.; Boubel, J. C.; Canet, D. *Mol. Phys.* **1997**, *90*, 399.
(10) Gauthier, L.; Robert, J. B.; Canet, D. *J. Mol. Liq.* **2000**, *85*, 77.
(11) Rozhdestvenskaya, N. B.; Smirnova, L. V. *J. Chem. Phys.* **1991**, *95*, 1223.
(12) Cabaço, M. I.; Danten, Y.; Besnard, M.; Guissani, Y.; Guillot, B. *J. Phys. Chem. B* **1997**, *101*, 6977.
(13) Tomasi, J.; Persico, M. *Chem. Rev.* **1994**, *94*, 2027.
(14) Frisch, M.; Trucks, G.; Schlegel, H.; Scuseria, G.; Robb, M.; Cheeseman, J.; Zakrzewski, V.; Montgomery Jr., J.; Stratmann, R.; Burant, J.; Dapprich, S.; et al. *Gaussian 98*; Gaussian Inc.: Pittsburgh, PA, 1998.
(15) Kisiel, Z.; Desyatnyk, O.; Pszczólkowski, L.; Charnley, S. B.; Ehrenfreund, P. *J. Mol. Spectrosc.* **2003**, *217*, 115.
(16) Williams, D. E.; Cox, S. R. *Acta Cryst. B* **1984**, *40*, 404.
(17) Rai, N.; Siepmann, J. I. *J. Phys. Chem. B* **2007**, *111*, 10790.
(18) Jorgensen, W.; Maxwell, D. S.; Tirado-Rives, J. *J. Am. Chem. Soc.* **1996**, *118*, 11225.
(19) Steele, W. V.; Archer, D. G.; Chirico, R. D.; Collier, W. B.; Hossenlopp, I. A.; Nguyen, A.; Smith, N. K.; Gammon, B. E. *J. Chem. Thermodyn.* **1988**, *20*, 1233.
(20) Barker, J. A.; Watts, R. O. *Mol. Phys.* **1973**, *26*, 789.
(21) Neumann, M. *J. Chem. Phys.* **1985**, *82*, 5663.
(22) Neumann, M. *J. Chem. Phys.* **1986**, *85*, 1567.
(23) Fincham, D. *CCP5 Inf. Q.* **1981**, *2*, 6.
(24) Allen, M. P.; Tildesley, D. J. *Computer Simulation of Liquids*; Oxford University Press: Oxford, 1987.
(25) Diez, E.; Bermejo, F. J.; Guilleme, J. *J. Chem. Phys.* **1985**, *83*, 58.
(26) Abragam, A. *Principles of Nuclear Magnetism*; Oxford University Press: Oxford, 1961.
(27) Gordon, R. G. *Adv. Magn. Reson.* **1968**, *3*, 1.
(28) Steele, W. A. *Adv. Chem. Phys.* **1976**, *34*, 1.
(29) Millot, C.; Soetens, J.-C.; Ahmad, N.; Adnan, R. *Europhys. Lett.* **2011**, *96*, 43002.
(30) Fu, C.-F.; Tian, S. *J. Chem. Theory Comput.* **2011**, *7*, 2240.